Acta Cryst. (1954). **7**, 733

An X-ray Study of the Substructure of Fine-grained Aluminum

By Sigmund Weissmann and Doris L. Evans

College of Engineering, Rutgers University, New Brunswick, New Jersey, U.S.A.

(*Received* 11 *January* 1954 *and in revised form* 26 *February* 1954)

Details of the grain substructure of fine-grained aluminum have been revealed by the X-ray double-crystal diffractometer by means of a multiple-exposure technique. The data obtained are used to compute statistical parameters that are a measure of the angular tilt between adjacent subgrains and of the angular misalignment of the lattice within a subgrain. An interpretation of the observed data as functions of lattice bending is presented.

1. Introduction and experimental technique

A number of investigators have shown that the breakdown of the X-ray patterns obtained upon annealing a metal deformed at room temperature is closely connected with the existence of a subgrain structure (Guinier & Tennevin, 1948; Crussard, 1944; Cahn, 1949–50; Dunn, 1946; Dunn & Daniels, 1951). Considerable controversy has arisen concerning the correctness of the postulated mechanism of subgrain formation (Wood & Rachinger, 1949–50) and therefore it was felt that an X-ray diffraction technique of high resolution might shed additional light on the nature of this process. Since the 'X-ray double-crystal diffractometer' has been employed to great advantage in the study of silicon powder, silicon ferrite and low-carbon steel (Reis, Slade & Weissman, 1951; Slade & Weissman, 1952) and has been proven to be sensitive to small modifications in lattice imperfections, this technique was chosen as the research tool in the present investigation.

The unique feature of this method is that the parallelized and monochromatized beam reflected from the first crystal irradiates the specimen, each reflecting crystallite of which may independently be considered to be the second crystal of the conventional double spectrometer. The reflections of the crystallites are recorded along the Debye–Scherrer curves of a cylindrical film having its center of curvature coincident with the axis of rotation of the test specimen. Discrete film shifts are made between each specimen position, thereby giving rise to a multiple-exposure diagram which is characterized by an array of spots for each reflecting crystallite. These arrays of spots are analogous to the rocking curves of single crystals and can be analyzed in a similar manner. For the measurement of the variation in spot intensity as a function of angular specimen setting a modified positive-print method has been employed (Evans & Weissman, 1953). The analysis of the intensity distribution curve of each array of spots yields statistical parameters which are a measure of the lattice imperfections of each crystallite. Since all the reflecting crystallites can be studied in such a manner, a representative sampling of the lattice imperfections of the total crystallite population can be obtained.

2. Experimental observations and analysis of data

Almost all the arrays recorded in previous studies of silicon powder and low-carbon steel exhibited intensity distributions that are adequately described by a

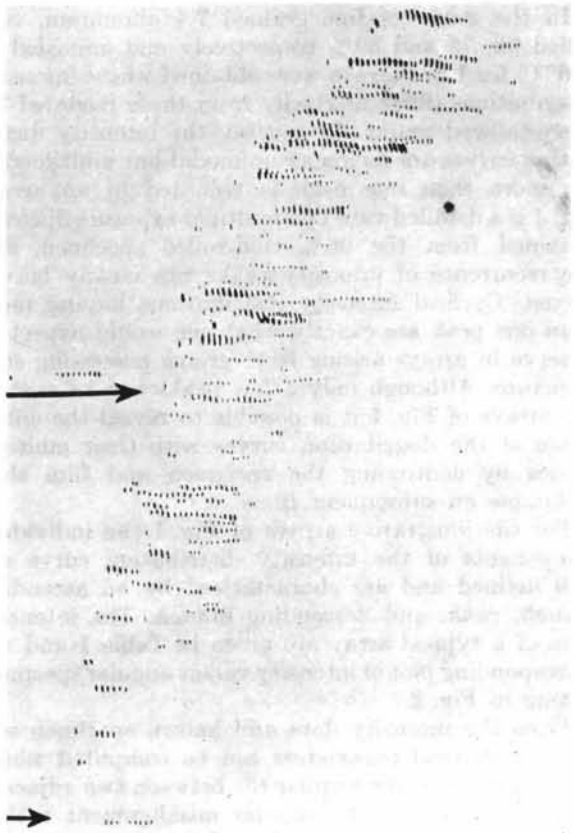

Fig. 1. Detailed view of (422) reflection of multiple-exposure diagram exhibiting multi-modal intensity distribution curves typical of subgrain structure. Aluminum specimen 99·95% pure, 96% reduced, annealed 1 hr. at 300° C. Specimen shifts: 4 minutes of arc.

Table 1. *Computation of the statistical parameters* $\bar{\varphi}$, $\Delta\varphi$, σ

99·95% Al, 96% cold rolled, annealed at 300° C. for 1 hr.
(222) line, (1, +1) position, equatorial reflection.

Angular specimen shift $\varphi = 4'$	Corrected integrated intensity I	ΣI	$I\varphi$	$\Sigma I\varphi$	$I\varphi^2$	$\Sigma I\varphi^2$	$\bar{\varphi} = \Sigma I\varphi/\Sigma I$	$\bar{\varphi}^2$	$\overline{\varphi^2} = \Sigma I\varphi^2/\Sigma I$	$\Sigma^2 = \overline{\varphi^2} - \bar{\varphi}^2$	Intensity data computed on the basis of normal probability curve
0	5		0		0						1·5
1	19	51	19	78	19	152	1·53	2·43	2·98	0·64	22·0
2	22		44		88						23·0
3	5		15		45						1·5
4	6		24		96						9·0
5	37		185		925						33·0
6	65		390		2340						60·0
7	54	192	378	1234	2646	8226	6·43	41·34	42·84	1·50	55·0
8	18		144		1152						26·0
9	7		63		567						7·0
10	5		50		500						1·0
11	5		—		—						
12	25		—		—						

$\Delta\varphi = 6{\cdot}43 - 1{\cdot}53 = 4{\cdot}90 \times (4') = 19{\cdot}6'$; $\sigma_1 = \{0{\cdot}64 \times (4')^2 - 169/3600\}^{\frac{1}{2}} = 3{\cdot}19'$; $\sigma_2 = \{1{\cdot}50 \times (4')^2 - 169/3600\}^{\frac{1}{2}} = 4{\cdot}90'$.

Gaussian distribution curve. This type of distribution function is characteristic of double-crystal diffractometer studies of recrystallized grains in which no substructure has been observed.

In the study of fine grained 7*A* aluminum, cold rolled 96, 75 and 50% respectively and annealed at 300° C. for 1 hr., arrays were obtained whose intensity distributions differ markedly from those recorded for recrystallized grains. In general, the intensity distribution curves are no longer unimodal but multimodal, i.e. more than one peak is recorded in an array. Fig. 1 is a detailed view of a multiple-exposure diagram obtained from the 96% cold-rolled specimen, and the recurrence of intensity peaks can clearly be observed. Cyclical intensity distributions having more than one peak are exactly what one would expect to observe in arrays arising from grains possessing substructure. Although only a few peaks can be seen in the arrays of Fig. 1 it is possible to reveal the entire range of the distribution curves with their multiple modes by continuing the specimen and film shift technique on subsequent films.

For the illustrative arrays of Fig. 1 the individual components of the intensity distribution curve are well defined and are characterized by an ascending branch, peak, and descending branch. The intensity data of a typical array are given in Table 1 and the corresponding plot of intensity versus angular specimen setting in Fig. 2.

From the intensity data and known specimen settings, statistical parameters can be computed which are a measure of the angular tilt between two adjacent subgrains and also the angular misalignment within the subgrain. If the means, $\bar{\varphi}_1$ and $\bar{\varphi}_2$ of two neighboring individual components of the distribution curve are determined as shown in Table 1, then the angle, $\Delta\varphi$, subtended by the means is the projected tilt of two adjacent subgrains (see Fig. 2). For the specific data quoted in Table 1, $\Delta\varphi$ was computed to be 19·6 minutes of arc.

In order to determine the angular misalignment existing within a subgrain, the standard deviation, σ, of the individual components of the distribution curve is computed. This statistical parameter is a measure of the lattice imperfection of the subgrain and thus gives information about the fine structure or mosaic spread of the subgrain. For the illustrative array quoted above the computation of σ is particularly simple since the reflections occur near the equator and the contribution of the vertical convergence of the beam to the rocking curve of the grain reflection is negligible.

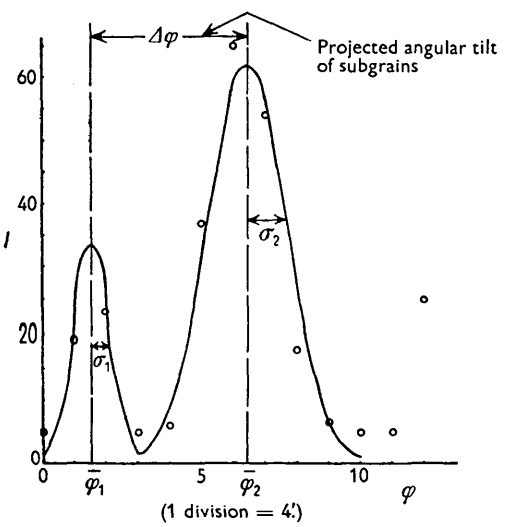

Fig. 2. Comparison of the experimental data and theoretical Gaussian intensity distributions for equatorial reflection of Al 96% cold rolled, annealed 1 hr. at 300° C. (222) line (1, +1) position. Circles: experimental data; full line: theoretical curve.

Equation (9) of Slade & Weissman (1952) therefore reduces to

$$\Sigma^2 = \sigma^2+\sigma_\eta^2 , \quad (1)$$

and, introducing the correction for the dispersion of the double-crystal diffractometer, which becomes significant only at large Bragg angles (Schwarzchild, 1928),* we obtain

$$\Sigma^2 = \sigma^2+\sigma_\eta^2+\sigma_D^2 , \quad (2)$$

where Σ^2 is the variance of the photometric intensities computed from the intensity data shown in Table 2.

σ_η^2 is the variance in the horizontal direction of the converging beam experimentally determined from the rocking curve of the first crystal. For the calcite crystal used $\sigma_\eta^2 = 169$ sec.^{2}.

$\sigma_D = \Delta\lambda D/2{\cdot}36$, where $\Delta\lambda$, the full width at half maximum of the radiation used, is 0·58 X. (Compton & Allison, 1935) for Cu $K\alpha_1$ and

$$D = (1/\lambda)\,[\tan\theta(\lambda, na)\pm\tan\theta(\lambda, nb)] .$$

In this expression λ is the wavelength under consideration, e.g. Cu $K\alpha_1 = 1537{\cdot}395$ X., and θ_a, θ_b and n_a, n_b represent the Bragg angles and the orders of reflection of the calcite crystal and the reflecting crystallite respectively. The selection of sign is determined by the position of the reflecting crystallite relative to the first crystal, the positive sign being taken for the arrays of the $(na, +nb)$ wing and the negative sign for those of the $(na, -nb)$ wing of the X-ray diagram.

It should be emphasized that the computations of the statistical parameters $\bar{\varphi}$ and α are perfectly general and are not based on any assumption as to the nature of the distribution function, the only requirements being the intensity data and the known specimen settings. The last column of Table 1 gives the intensity data which are to be expected if the individual components of the multi-modal distribution curve were to follow a normal probability function. It can be seen that a fairly good agreement exists between the observed and computed data and hence the intensity distribution of the individual components can be considered to follow a Gaussian error curve to a first approximation.

The intensity distribution of the arrays of spots off the equator is systematically modified by the increasing influence of the convergence of the beam. For these arrays the statistical parameters are computed with the aid of equation (9) of Slade & Weissman (1952). This equation expresses the systematic variance of the photometric intensities.

The range of $\Delta\varphi$ and σ values computed for all the specimens analyzed are listed in Table 2. These values were computed from data obtained for various (hkl) reflections. It will be observed that for a given annealing temperature the degree of cold rolling influences the tilt between adjacent subgrains and the lattice imperfection within a subgrain. The increase of $\Delta\varphi$ and σ with cold rolling is in agreement with results obtained by previous authors using other techniques (Hirsch & Kellar, 1952; Delisle, 1953*a*, *b*).

Table 2. *Dependence of subgrain parameters as a function of cold rolling*

(All angles are in minutes of arc)

Percentage cold rolling	Spread of $\Delta\varphi$	$\Delta\varphi$ most frequently observed	Spread of σ	σ most frequently observed
50	6–14	8	2–4	3
75	6–16	10–12	4–6	5
96	12–28	16–18	4–12	6–8

The dimensions of the analyzing beam and the limit of its resolving power are such that arrays are observed for which the minimum intensity between adjacent peaks does not fall to the level of the background. The peaks of the distribution are clear, however, and the observed array can be decomposed, by graphical means, into its individual elements since the Gaussian nature of these components has been established.

It is apparent that the evidence of the break up of the grains into subgrains should be observable in all directions along the Debye–Scherrer curves and not only in the horizontal direction for which the sequence of subgrains has been clearly established by the multimodal distribution curve. One can indeed observe a clustering and partial interpenetration of the arrays of spots in certain regions of the Debye–Scherrer curves which adds to the complexity of analysis. It can, however, be shown that the angular separation of adjacent arrays clustered in the vertical direction is of the same order of magnitude as the angular tilt of the subgrains when computed from the means of the multimodal distribution curve. This consistency in the magnitude of the angular separation of the reflections in all directions of the Debye–Scherrer curve is demonstrated with the aid of equation (11) of Reis, Slade & Weissman (1951):

$$\sin\Psi = \frac{y/R}{2\sin\theta[1+(y/R)^2]^{1/2}} , \quad (3)$$

where θ is the Bragg angle, Ψ is the latitude of the normal of the reflecting planes on the unit sphere of reflection, y is the vertical film distance of the reflection measured from the equator and R is the camera radius.

What we now wish to compute is the variation in latitude $\Delta\Psi$ which corresponds to the small vertical separation dy measured between adjacent arrays in a cluster. Differentiating (3), one obtains

* This equation expresses in terms of variance the usual Schwarzchild equation. Variance is used instead of half-width since the relation between the variances is independent of the analytical forms of their respective intensity distributions and therefore no assumption concerning the Gaussian nature of these distributions is implied.

$$\cos \Psi \Delta\Psi = \frac{1}{2 \sin \theta} \left\{ \frac{1/R}{[1+(y/R)^2]^{1/2}} - \frac{y^2/R^3}{[1+(y/R)^2]^{3/2}} \right\} dy \,, \tag{4}$$

and, substituting from (3),

$$\Delta\Psi = \frac{dy}{y[1+(y/R)^2]} \tan \Psi \,. \tag{5}$$

For reflections near the equator, where $\cos \Psi \sim 1$, equation (4) reduces to

$$\Delta\Psi = dy/2 \sin \theta R \,. \tag{6}$$

Equations (5) and (6) were used to compute $\Delta\Psi$ for clusters of arrays along several (*hkl*) reflections. Values were obtained which are of the same order of magnitude as the values of $\Delta\varphi$ obtained from the horizontal multi-modal intensity distribution; a consistency which clearly points to subgrain formation as the operating mechanism.

3. Relation of observed substructure to lattice bending

A careful scrutiny of the geometrical pattern of spot sequence in the multiple-exposure diagram yields information concerning the mechanism of substructure formation. It may be observed in Fig. 1 that the sequences of spots pertaining to adjacent subgrains do not fall on the same straight line but are slightly tilted with respect to each other. This phenomenon can be properly explained if we consider the geometrical conditions necessary for X-ray reflection.

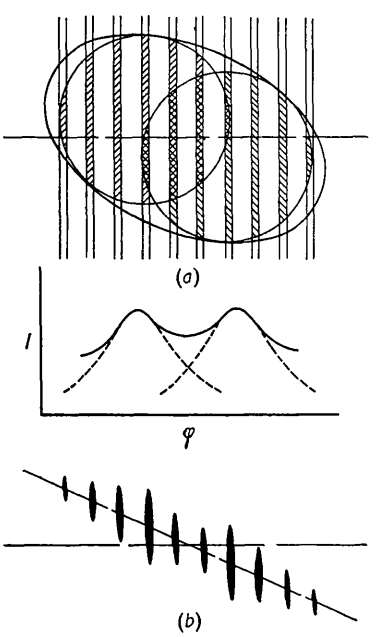

Fig. 3. Relation between array of spots and the geometry of reflection at the equator for adjacent subgrain domains. (*a*) Representation of region of misaligned subgrain normals and advancing reflecting zone. (*b*) Resulting array of spots and plot of its bi-modal intensity distribution.

It was shown by Slade & Weissman (1952) that X-ray reflection occurs when the region of misalignment in the unit sphere, representing the misorientation within the crystallite, intersects the reflecting zone. For a completely recrystallized strain-free grain in which no substructure is observed the point density of normals in the region of misalignment is a two-dimensional Gaussian with a mean at the Bragg angle. In this isotropic case the region of misalignment is bounded by a circle of constant minimum observable density.

If, however, the grain is strained by bending, the isopycs of the Gaussian are ellipses since the variance is larger in the plane of bending than in the plane perpendicular to it.

In the process of subgrain formation the bent grain is broken up into smaller and more perfect lattice elements and this mechanism can be schematically represented by the fragmentation of the ellipse into circular parts. Owing to the observed superposition of the intensity distribution from regions of adjacent subgrains, the circular components of the ellipse are represented as intersecting each other (Fig. 3(*a*)). The resulting geometrical diffraction pattern is depicted in Fig. 3(*b*). To facilitate the graphical representation of the reflecting conditions, the region of misalignment is kept stationary on the unit sphere and the reflecting zone is shown to move through it. It should be noted that this graphical representation of the postulated mechanism bears a striking resemblance to the actual diffraction patterns observed in Fig. 1, thus indicating that lattice bending is a prerequisite of subgrain formation.

Conclusion

The evidence of substructure for fine grained aluminum was manifested in the form of a multi-modal intensity distribution curve expressed as a function of angular specimen settings. Analysis of the distribution curve, based on statistical moment computations, yielded the following results: (1) For a given temperature of annealing, the angular tilt of adjacent subgrains increases with increasing cold-rolling. (2) The lattice imperfection within a sub-grain also increases with increasing cold rolling. (3) A model that relates subgrain formation to lattice bending is proposed on the basis of analysis of the observed X-ray reflections.

The authors wish to express their gratitude to the Office of Naval Research and the Office of Ordnance Research, U.S. Army, for the support of this work, and to Prof. J. J. Slade, Jr. for numerous helpful discussions during the course of these studies. The specimens used were obtained through the kind co-operation of Dr A. H. Geisler of the General Electric Company.

References

CAHN, R. W. (1949–50). *J. Inst. Met.* **76**, 121.
COMPTON, A. H. & ALLISON, S. K. (1935). *X-rays in*

Theory and Experiment, table IX–21. New York: van Nostrand.
CRUSSARD, C. (1944). *Rev. Métall.* **41**, 114.
DELISLE, L. (1953*a*). *J. Metals, N.Y.* **5**, 5.
DELISLE, L. (1953*b*). *J. Metals, N.Y.* **5**, 660.
DUNN, C. G. (1946). *Trans. Amer. Inst. Min. (Metall.) Engrs.* **167**, 373.
DUNN, C. G. & DANIELS, F. W. (1951). *Trans. Amer. Inst. Min. (Metall.) Engrs.* **191**, 147.
EVANS, D. L. & WEISSMANN, S. (1953). *J. Opt. Soc. Amer.* **43**, 1183.
GUINIER, A. & TENNEVIN, J. (1948). *C. R. Acad. Sci., Paris*, **226**, 1530.
HIRSCH, P. B. & KELLAR, J. N. (1952). *Acta Cryst.* **5**, 162.
REIS, A., SLADE, J. J. & WEISSMANN, S. (1951). *J. Appl. Phys.* **22**, 665.
SCHWARZCHILD, M. (1928). *Phys. Rev.* **32**, 162.
SLADE, J. J. & WEISSMANN, S. (1952). *J. Appl. Phys.* **23**, 323.
WOOD, W. A. & RACHINGER, W. A. (1949–50). *J. Inst. Met.* **76**, 730.

Acta Cryst. (1954). **7**, 737

The Crystal Structure of Ximenynic Acid

BY O. A. TESCHE

Department of Physics, University of Cape Town, South Africa

(*Received* 13 *March* 1954 *and in revised form* 28 *May* 1954)

An attempt to determine the crystal structure of ximenynic acid is described. The main findings are:

The crystals are triclinic ($P\bar{1}$). $Z = 2$.

There is a tendency for the molecule to form a straight carbon chain, as in other simpler fatty acids, but the presence of the triple and double bonds prevents this to a certain extent.

The double bond carries its attachments in the *trans* position. The spatial arrangement of the double-bond group presents an unexpected feature.

Ximenynic acid is a conjugated unsaturated monobasic fatty acid with the bulk formula $C_{18}H_{30}O_2$ isolated by Ligthelm & Schwartz (1950) from kernels of *Ximenia Caffra*. According to Ligthelm, Schwartz & von Holdt (1952), the structural formula of the acid is

$$COOH.(CH_2)_7.C\vdots C.CH:CH.(CH_3)_5.CH_3$$

and examination of the infra-red absorption of methyl ximenate by Ahlers & Ligthelm (1952) indicates the possibility of a *trans* configuration of the double bond.

An X-ray examination of crystals of the acid was undertaken to determine (*a*) whether the molecule of the acid is straight or whether it bends back on itself at the double bond, and (*b*), whether the bond is of the *cis* or *trans* type, the two questions being of course related. It has not been possible in the time available to make a complete determination of the structure, but its general nature is clear and a definite answer can be given to the stereochemical questions.

The crystals available were very thin white plates, oblong in shape and showing no definite faces except those of the plates themselves. X-ray examination showed one important axis—later called the *b* axis—to lie parallel to the long axis of the plates. A second axis, *a*, was found to lie in the plate. Oscillation photographs gave the axial lengths

$$a = 4{\cdot}634 \pm 0{\cdot}032 \text{ Å}, \quad b = 5{\cdot}572 \pm 0{\cdot}004 \text{ Å},$$

with $\gamma = 84° 51'$.

The determination of the *c* axis is less easy owing to the thinness of the plates. The area $ab \sin \gamma$ is 25·7 Å^2, which is greater than the cross-sections of the known fatty acids, which are of the order of 18 Å^2. On the other hand, it is not large enough for a chain doubled back on itself. The figures suggest that the *c* axis will be a long one, inclined at a considerable angle to the plane of the plates.

The (001) *spacing* can be determined at once from an oscillation photograph. It is 34·20±0·13 Å, and the unit cell has a volume 879 Å^3. The molecular weight of the cell is 278·2 and the density 1·04 g.cm.$^{-3}$. There are two molecules in the unit cell.

Oscillation photographs taken about an axis perpendicular to the plate, and therefore parallel to the c^* reciprocal axis, show row-lines, closely set with points. By taking such photographs with the rays travelling along the *a* and the *b* axes it is possible to estimate the directions of valid a^* and b^* axes and so to determine the direction of a possible *c* axis. The *c* axis first determined was that lying most nearly perpendicular to the *ab* face. It was 34·4 Å in length with a cross-section of 25·7 Å^2, and was therefore probably not the structural unit cell. Photographs showed the 016 spectrum referred to the cell to be very strong and to be accompanied by very well marked, nearly circular, thermal diffuse spots. This indicates that the plane (016) is probably parallel to the direction of the acid chains, and, as a result of considerations of this kind, a cell